

In Situ Study of Peritectic Couple Growth Under Purely Diffusive Conditions



ANDREAS LUDWIG and JOHANN MOGERITSCH

Herein, in a microgravity campaign onboard the International Space Station, peritectic coupled growth (PCG) is studied by solidifying alloys of the peritectic transparent organic system TRIS–NPG under purely diffusive conditions. The experiment reveals that the formation of PCG begins with coagulated lateral bands comprising the peritectic phase at temperatures below the peritectic one. After reaching the growth front of the pro-peritectic phase, growth competition between both solid phases occurs such that the patches of the pro-peritectic phase, lamellae, and fibers/rods grow in the stated order, coupled with the peritectic phase. As the entire solidification process occurs during the initial transient stage, the diffusion coupling between the two solid phases is weak. With the gradual decrease in the interface temperature during the initial transient, the necessary growth conditions for the pro-peritectic phase diminish. Additionally, different concentrations along the inclined solid/liquid interface favor the peritectic phase at the rear window and the pro-peritectic phase at the front window. The corresponding PCG lasts 19 hours while the recoil of the inclined interface continues to a temperature level that makes alterations of the ‘effective’ TRIS–NPG phase diagram necessary.

<https://doi.org/10.1007/s11661-023-07052-6>
© The Author(s) 2023

I. INTRODUCTION

PERITECTIC alloys can form eutectic-like two-phase microstructures under certain conditions. This microstructure develops through peritectic coupled growth (PCG), like the well-known eutectic coupled growth (ECG). The first experimental evidence of PCG was found in 1973 by Fisher and Kurz for the Sn–Sb alloy system (presented in Reference [1]). In the 1990s, further evidence of this peculiar growth form was reported: Lee and Verhoeven for the Ni–Al system,^[2] and Vandyoussefi *et al.* for the Fe–Ni system.^[3,4] Subsequently, Lo *et al.*^[5] and Dobler *et al.*^[6] further investigated PCG in the Fe–Ni system and Valloton *et al.* in the Cu–Sn system.^[7] A necessary condition for lamellar PCG is that the primary, pro-peritectic phase should grow with a velocity close to or even slightly above the critical value for morphological stability,^[6] which is often much lower than 1 $\mu\text{m/s}$ (or 3.6 mm/h). Because low-growth velocities are seldom used, eutectic-like two-phase microstructures in peritectic alloys do not appear in general processing routes.

Chalmers predicted PCG in 1959^[8,9] and postulated that isothermal PCG should be possible for hypo-peritectic alloys, ranging from the primary to the peritectic phase. Later, a large thermal gradient was reported necessary for the PCG to suppress the dendritic/cellular growth of the pro-peritectic phase.^[10,11] In 1974, Boettinger studied the occurrence of alternating bands in peritectic systems^[12] and applied the standard Jackson–Hunt model for eutectic growth^[13,14] to peritectic systems. Simultaneously, diffusive band formation was understood,^[15] and its dependence on the oscillatory modes of convection was clarified.^[16,17] In small-diameter samples, where convection is suppressed, bands were formed by alternate nucleation and lateral growth of the two solid phases.^[15,16] In addition, the formation of partial bands, called island banding, was observed. Phase-field simulations predicted that island banding leads to PCG if the spacing between islands is within a stable range of lamellar spacings.^[5] However, nucleation must be sufficiently facile for this phenomenon to occur.

A direct *in-situ* observation of PCG formation in a thin sample of 600 μm spacing with solutal buoyancy flow in TRIS–NPG alloys (TRIS–tris (hydroxymethyl)aminomethane and NPG–neopentyl glycol) was previously reported in 2017.^[18] Both organic

ANDREAS LUDWIG and JOHANN MOGERITSCH are with the Department Metallurgy, University of Leoben, 8700, Leoben, Austria. Contact e-mail: ludwig@unileoben.ac.at

Manuscript submitted January 19, 2023; accepted April 3, 2023.

Article published online April 26, 2023

compounds exhibit a high temperature “plastic crystal” formed by so-called “globular molecules”.* These

*Such “globular molecules” might physically not be 100 pct spherical, but they reveal the characteristic rotational freedom so that they solidify metal-like.

molecules undergo phase transitions from a lower temperature-ordered structure (orthorhombic for TRIS and monoclinic for NPG) to a higher temperature orientationally disordered phase (bcc for TRIS and fcc for NPG), referred to as “plastic crystal phase” or “orientationally disordered crystal (ODIC)”. Lower temperature-ordered phases typically appear needle-like as they grow as faceted crystals. Conversely, ODIC forms cellular and dendritic morphologies, like those of solidifying metals or alloys.

The TRIS–NPG phase diagram was experimentally determined by Barrio *et al.*^[19] and later confirmed by other studies.^[20,21] Figure 1 shows a part of the TRIS–NPG phase diagram relevant to the present work. The peritectic invariant reaction, $\alpha + L \leftrightarrow \beta$, is located at $T_p = 410.7$ K and $c_p = 51$ mol pct NPG. Here, α is the primary pro-peritectic phase, and β is the peritectic phase. The (high temperature) eutectoid invariant reaction, $\alpha \leftrightarrow \beta + O$, which involves the TRIS-rich orthorhombic phase (O), is located at $T_{e1} = 392.5$ K and $c_{e1} = 43$ mol pct NPG. The second eutectoid invariant reaction, $\beta \leftrightarrow O + M$, at $T_{e2} = 310.5$ K and $c_{e2} = 96$ mol pct NPG, involves the NPG-rich monoclinic phase (M), which is not relevant to this study. Figure 1 also shows the metastable extensions of the liquidus and solidus lines for α and β estimated by a re-optimized CALPHAD approach for the TRIS–NPG system.^[22]

The objective of this study was to describe direct observations of the dynamics of PCG formation, without the interfering influence of convection, using near-peritectic TRIS–NPG alloys during microgravity solidification experiments onboard the International Space Station (ISS). A specific experiment was selected to observe PCG with sufficient optical quality. Findings from other experiments in the same microgravity (μg) campaign^[23,24] will occasionally be mentioned.

II. EXPERIMENTAL PROCEDURE

Between March 17 and April 24, 2021, three cartridges filled with TRIS–NPG alloys of near-peritectic compositions were used for studies on PCG onboard the ISS.^[23,24] Each cartridge was conceptually separated into six segments that were individually processed. A typical experiment began with sample annealing for 1 hour at an elevated temperature (without visible traces of molten areas) to equilibrate the microstructure and completely dissolve the faceted low temperature phases. Then a segment was held for 2 hours in a predefined temperature gradient, and the cartridge was pulled at a constant velocity while maintaining the gradient. By processing each segment in this manner, the used

segments, located in regions of higher temperatures, melted, whereas the unused segments did not melt before processing. The experiments were performed with the “Transparent Alloy” (TA) facility, an insert in the Microgravity Science Glove-Box (MSG), which was developed by QinetiQ Space** (Antwerp, Belgium) on

**<https://www.qinetiq.com/en/sectors/space> recently changed to be part of <http://www.redwirespace.eu/>

behalf of the European Space Agency (ESA).^[25] The optical recording system of the TA apparatus included a light-emitting diode array as light source and a CCD camera with a field of view (FOV) of 6.1×5.1 mm² centered at the adiabatic zone. Images were acquired at the three focus points: $ff_1 = 0$ mm (directly at the front glass wall); $ff_2 = 0.5$ mm (at the center of the cartridge); and $ff_3 = 0.8$ mm (near the rear glass wall).

The organic compounds used were supplied as powders with purities of > 99.9 pct for TRIS and > 99 pct for NPG. NPG was dried for 24 hours at 378 K to reduce its water content. TRIS was used without further processing as it is sensitive to long-term annealing in the liquid state. The alloy was prepared in an inert gas atmosphere by mixing powders of both organic compounds in a container and melting them. The container was sealed during the process owing to the low vapor pressure of the NPG. After cooling the material to room temperature, the alloy was ground into millimeter-sized parts and stored in a closed container for later use. The materials were melted again using a specially constructed furnace and then sucked into a special syringe. Subsequently, the material was shipped to QinetiQ Space in a sealed plastic bag filled with argon, and the cartridges for space experiments (TAC) were filled and later leak-tested. The cartridges had a solidification volume of 100 (length) \times 6 (width) \times 1 mm (depth). Owing to the specific requirements for the contact area between the cartridge and the hot and cold clamps, the effective solidification length was 66 mm. As mentioned above, this length was conceptually divided into six segments of 11 mm each. The solidification experiments were conducted only on ‘fresh’ segments that had not yet been melted.

The experiment reported here was performed with the second segment of TA-cartridge four, named TAC4s2. It was processed between April 19, 2021, 06:32 GMT, and April 20, 2021, 11:30 GMT. The clamp temperatures were $T_{hot} = 439$ K and $T_{cold} = 379$ K, and the pulling rate was set as $V_{pull} = 0.360$ mm/h.

III. RESULTS

At the beginning of the 2 hours gradient stage, the material appeared to consist of 10–20 μm fine polycrystalline grains, which immediately melted on the hot side of the FOV. Grains close to the molten area were surrounded by melt (mushy region). During the progression of the gradient stage, the mushy/liquid (m/l)

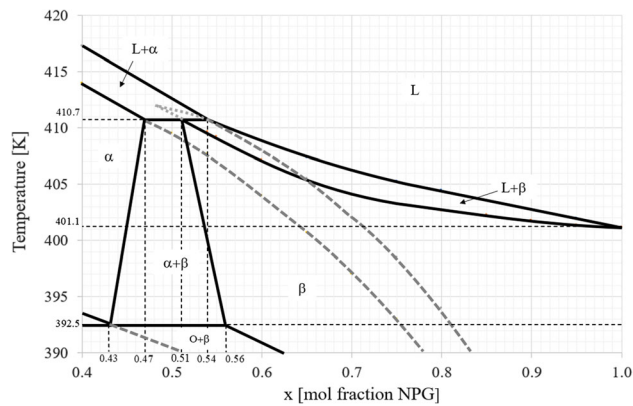


Fig. 1—Relevant part of the TRIS–NPG phase diagram according to the measurements by Barrio *et al.*,^[19] completed with the metastable extension of the α - and β -liquidus and solidus lines according to the CALPHAD dataset presented in Ref. [22] The peritectic and the high-temperature eutectoid invariants are specified together with the melting point of the β -phase when containing 100 pct NPG. The phase regions are labeled based on the equilibrium diagram. “Reprinted from Ref. [22] under CC BY 4.0”.

interface recoiled, whereas the grain coarsened and grain boundaries migrated toward the m/l interface (TGZM).^[22,26–28] After the gradient stage, the m/l interface was slightly convexly curved at a distance from the right (hotter) edge of the FOV (1.12 mm for the upper and lower parts and 1.18 mm for the central part of the front interface). Furthermore, the m/l interface was unintentionally inclined with the foremost grains at the front window and the backdropped grains near the rear window, which was the starting point of the solidification experiments.

Figure 2 shows how the interface position changed during the experiment. After 22 hours of pulling, the sample was kept stationary in the gradient for 4 hours. The position of the interface at the front window was measured at the upper and lower edges of the FOV, and the center. The corresponding interface positions in the rear window could only be measured accurately after 3 hours of growth. Thus, the corresponding curves began only after 3 hours. The interface inclination increased with time from approximately 0.2 mm to 0.5 mm at the end of the pulling. In the first hour of pulling, solidification occurred at a growth velocity of $V_{\text{growth}} = 0.160$ mm/h. Between 5 and 22 h of pulling, the growth velocity was nearly constant at $V_{\text{growth}} = 0.236$ mm/h, which was approximately 66 pct of the pulling velocity ($V_{\text{pull}} = 0.360$ mm/h). Thus, the interface never reached steady-state conditions. At the end of pulling, the interface positions decreased again by 2–3 mm. Additionally, the inclination was reduced from 5 to 3 mm.

Figure 3 shows the dynamics of PCG formation at the center of the solid/liquid (s/l) interface. After 2 hours of growth, several lateral bands appeared in the lower temperature region. In Figure 3(a), a lateral band is marked in blue. The image shows an inclined polycrystalline s/l interface. However, the appearance of the

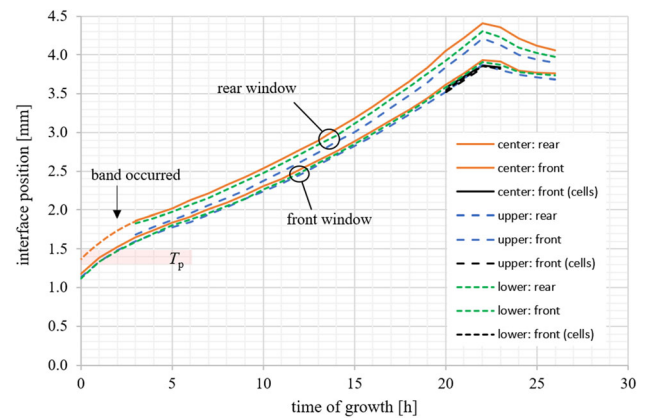


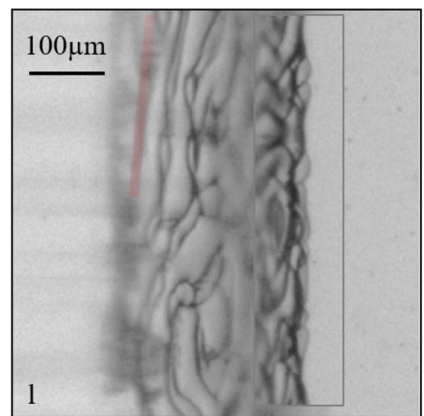
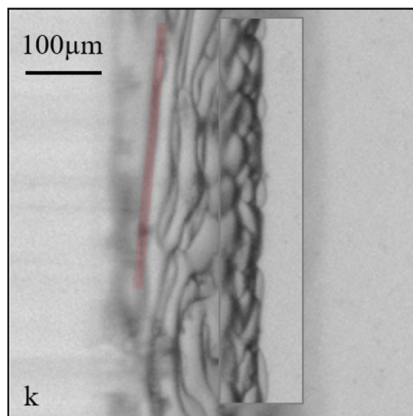
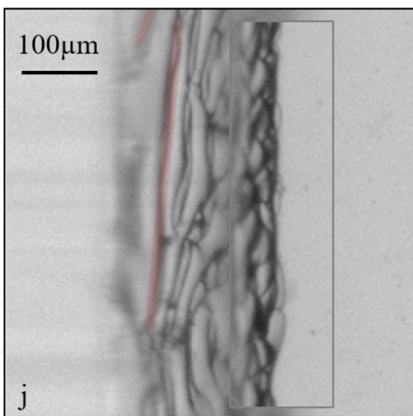
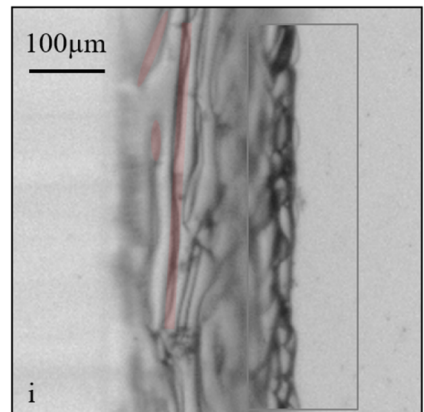
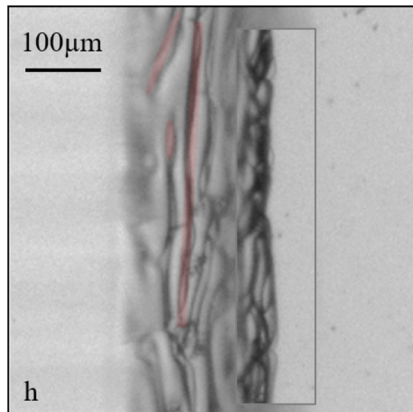
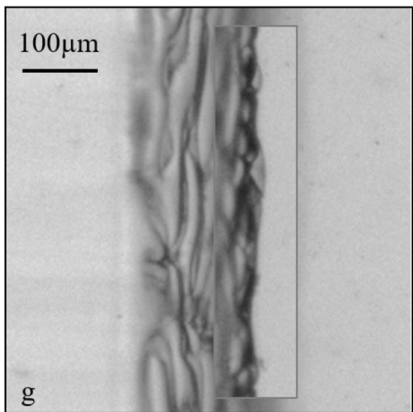
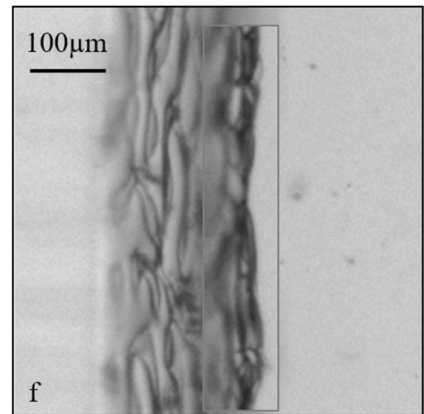
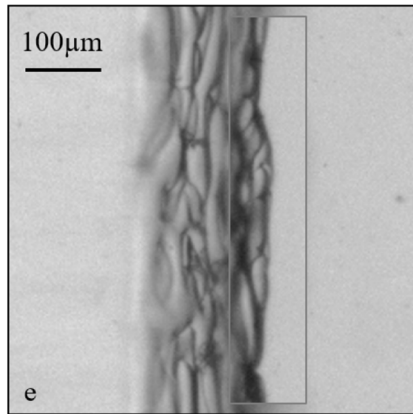
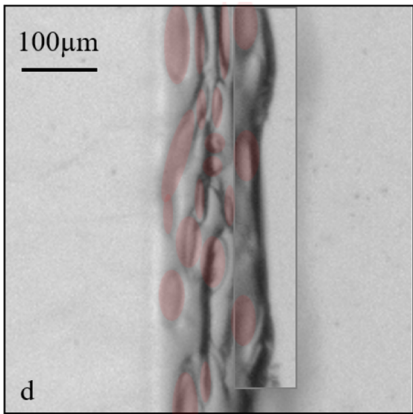
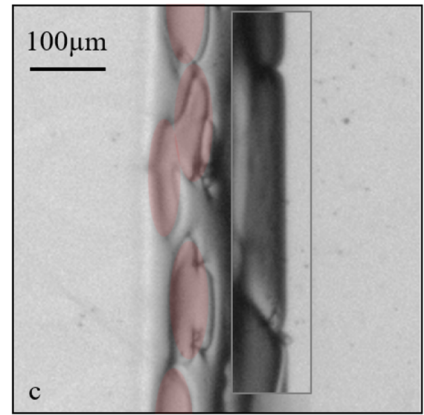
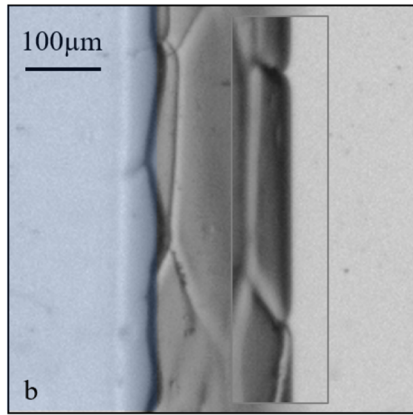
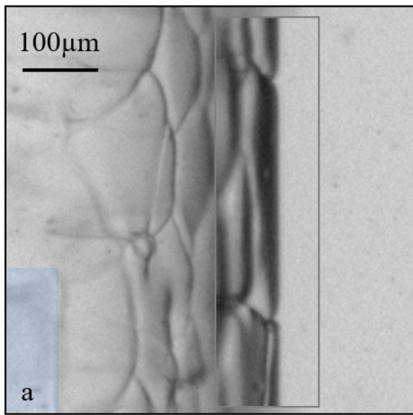
Fig. 2—Measured interface position of TAC4s2 from right-hand side of FOV as a function of solidification time. Given are the positions at the front window measured at the upper and lower edges of the FOV, and the center for both the interfaces at the front and rear window. After 20 hours, cellular growth occurs at the front window, as indicated by the black curves. After 22 hours of growth, pulling is stopped.

foremost grains at the back and the backmost grains at the front is an optical illusion. Essentially, the foremost grains were at the front window, and backdropped grains were observed through the 1 mm thick transparent material.

Figure 3(b) shows that the coagulated lateral bands reached the lower part of the s/l interface and began to travel along the inclined interface from the rear toward the front window. In Figure 3(c), this overgrowth was only partly as patches of the former s/l interface, marked in red, remained. Note that phase identification is not possible from only the pictures. In the discussion section, arguments to identify the polycrystalline interface consisting of the pro-peritectic α -phase and the band of the peritectic β -phase are presented.

A comparison of Figures 3(c) through (e) reveals that the phase patches decomposed into smaller areas and further into thin lamellae. Therefore, both α and β solid phases grew simultaneously from the melt, and PCG was established. This PCG continued for the rest of the experiment; thus, the segment TAC4s2 exhibited PCG for 19 hours. During these 19 hours, the interface recoiled by approximately 2.5–3 mm, as shown in Figure 2. In Figures 3(h) through (l), some specific lamellae are marked in red. One appeared extremely long, with a length of approximately 400 μm and width of only 20–30 μm . However, most lamellae at this stage were shorter and exhibited some necking. With the help of the red lamellae, the lamellae were observed to shift toward the lower part of the interface.

In Figure 4, the image sequence of Figure 3 continues. The elongated lamellae changed into a stage where the lamellae became more curved (Figures 3(l) and 4(a)–(c)). At the end of this stage, the second phase grew rod-like (Figures 4(f) through (h)). When pulling was stopped, these rods thickened and flattened, as shown in Figures 4(i) and (j).



◀Fig. 3—Dynamic of PCG formation and growth for TAC4s2. Pulling begins at 09:33 GMT. Picture (a) is acquired at 11:33 GMT, and the subsequent pictures are acquired 1 h later each. In (a) and (b) a lateral band comprising the peritectic phase is marked in blue, whereas the patches and selected lamellae of the pro-peritectic phase are marked in red. The pictures are acquired with focus at the center, except the insets, which are taken with front focus. The insets replace the blurry part of the picture taken with focus at the center. Pictures with focus near the rear window do not give further details (Color figure online).

IV. DISCUSSION

A. Temperature Distribution Inside the Cartridge

Information on the temperature distribution along the cartridge axis is required to interpret the results obtained. However, no direct temperature measurements were performed inside the cartridges, and only the temperatures of the hot and cold clamps were available. Therefore, realistic assumptions and indirect observations were made. During the construction phase of the TA furnace, QinetiQ Spaces performed temperature measurements inside cartridges that were similar to the ones in this study. The cartridges were filled with different organic materials and processed at different temperatures. Evidently, a sigmoidal function could express the temperature distribution from cold to hot with two unknown parameters: the center position and transition width of the sigmoidal function.

In this study, a specific experiment was performed to estimate these two unknown parameters. By gradually adjusting the cold- and hot-clamp temperatures, the position change occurring during the transition between complete darkness and partial transparency was measured. This transition can be attributed to the phase transition $O + \beta \rightarrow \alpha + \beta$ at $T_{e1} = 392.5$ K (see Figure 1) and is independent of concentration if $c_0 \leq 56$ mol pct NPG. However, the concentration of the segment used for this calibration (TAC4s6) might have been slightly higher, such as $c_0 = 58$ mol pct NPG. Even though this higher concentration was accounted for, the corresponding temperature information should be interpreted cautiously. Consequently, the temperature accuracy was considered as ± 1 K or slightly higher. The temperature curves shown in Figure 5 were obtained for two different estimated concentrations of the segment TAC4s6. In particular, the lower curve is an approximate temperature distribution for the present experiment. Thus, the peritectic temperature, T_p , was predicted to be located at $z = 1.4 \pm 0.1$ mm measured from the right edge of the FOV. This assumption is illustrated in Figure 2.

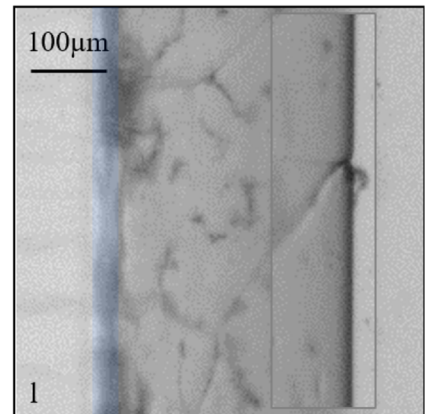
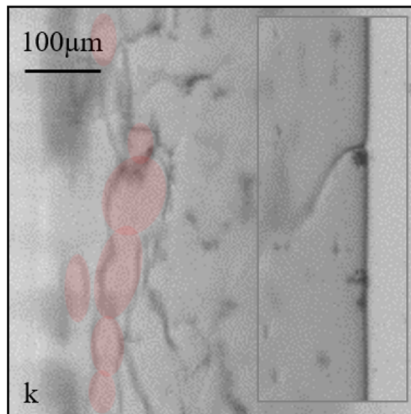
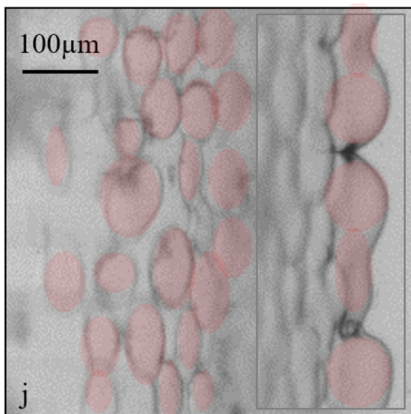
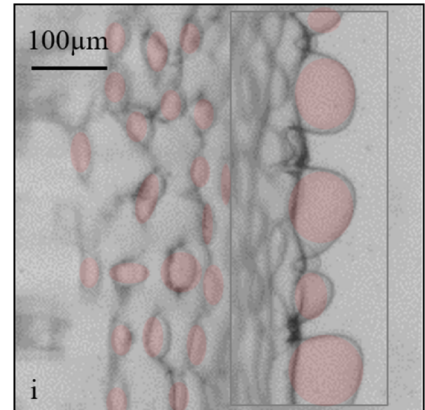
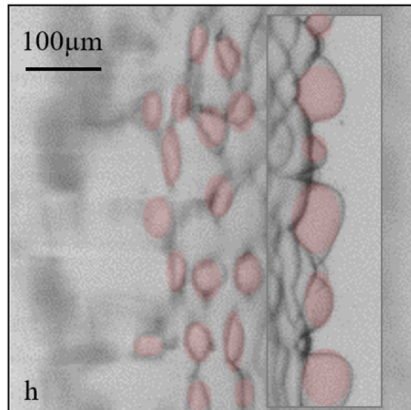
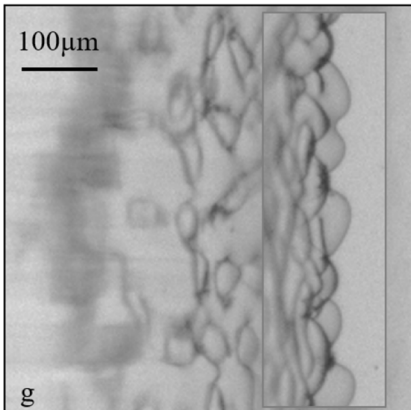
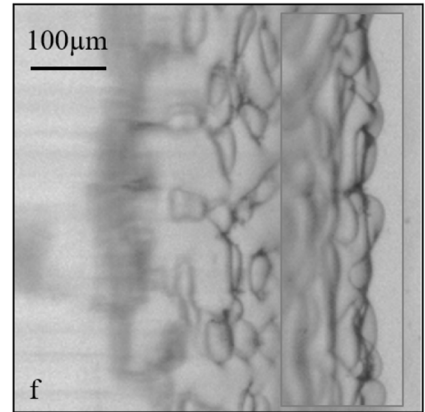
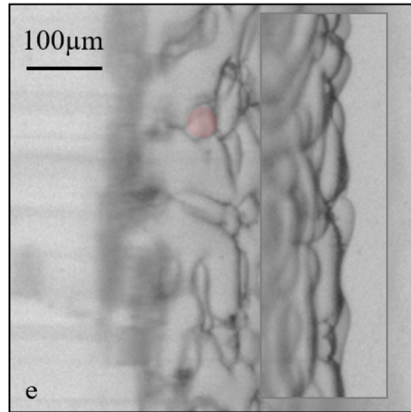
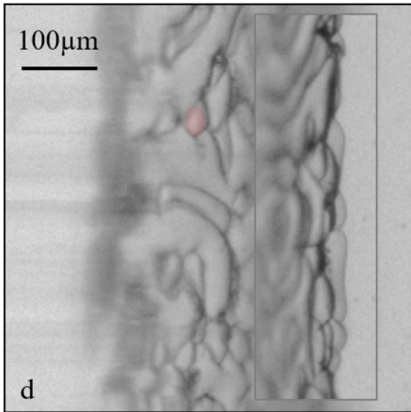
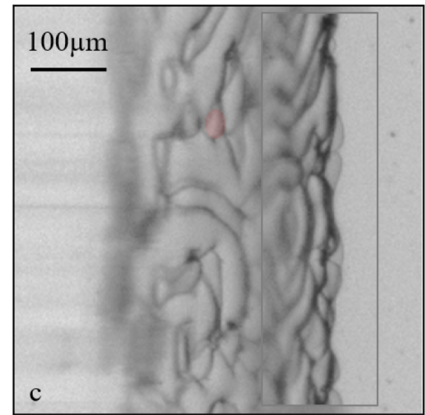
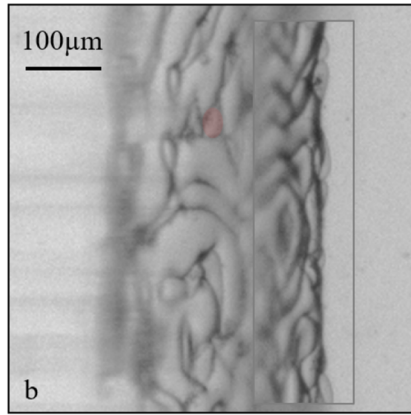
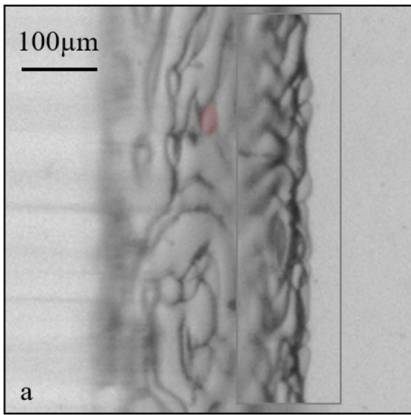
B. Alloy Composition of the Segment

Using the temperature distribution inside the cartridge, the position of the liquidus temperature could be determined to obtain information on the segment composition. Note that the liquidus temperature is determined by the initial position of the m/l interface following the establishment of the gradient. The m/l

interface at the end of the gradient stage was located at a distance from the right edge of the FOV (1.12 mm for the upper and lower parts of the front interface, and 1.18 mm for the central part). However, during the 2 hours gradient stage, grain boundary migration by TGZM slightly increased the concentration at the m/l interface.^[22] From a statistical analysis of the 18 experiments performed during the present μ g campaign, an approximate displacement of 0.14 ± 0.11 mm was estimated for the TGZM displacement during the gradient stage. Thus, the interface positions must be corrected to achieve 0.98 ± 0.11 mm for the upper and the lower part of the front interface, and 1.04 ± 0.11 mm for the central part to obtain the correct position of the segment's liquidus. From Figure 5, the temperatures that correspond to these positions were 412.7 ± 0.5 K and 412.5 ± 0.5 K. This inaccuracy was caused by the variance in the assumed TGZM displacement. However, the inaccuracy in the temperature approximation (± 1 K) was even larger. Nevertheless, the temperature difference between the upper and lower parts and the center of the curved m/l interface was relatively small. The temperature of the curved interface was completely above T_p , and the corresponding grains could be considered as α grains. From the given temperatures in the phase diagram (Figure 1), the segment composition at the front window was determined to be $c_0 = 50 \pm 1$ mol pct NPG. However, the nominal composition of the cartridge was 53 mol pct NPG. Evidently, the segments that were processed first (namely s1-s3) exhibited a lower composition, whereas segments that were processed later (e.g., s6) exhibited a higher composition compared with that of the nominal one. This is likely caused by creeping solutal buoyancy flow during solidification after leak testing on Earth.

C. Initial Interface Inclination

As all eighteen solidification experiments of the present μ g campaign showed an inclined interface with the foremost and the backmost m/l interface at the front and rear window, respectively, a thermal bias must be stated for the TA-facility. The fact that the initial inclinations are similar for all segments makes it is less likely that the intended buoyancy flow during leak testing caused them. Figure 2 shows that the backmost interface was located approximately 0.2 mm behind the foremost m/l interfaces at the beginning of pulling. According to Figure 5, this corresponds to a temperature difference of approximately 1 K; the same order of magnitude as the suggested temperature accuracy (± 1 K). Nevertheless, due to the thermal bias, an interface that is inclined in the described way should be considered as isothermal. With an initial position at 1.18 mm for the foremost and 1.38 mm for the backmost interface at the center of the FOV, the interface temperature of the inclined interface must be assumed to be between 411.8 ± 1 K and 410.9 ± 1 K. However, this result should be considered cautiously as all the measurements exhibited large uncertainties.



◀Fig. 4—Dynamic of PCG formation and growth for TAC4s2 (continuation). The pictures are taken subsequently to those of Fig. 3; essentially, (a) is acquired at 23:33 GMT and the subsequent pictures are acquired 1 hour later each. Selected rods of the pro-peritectic phase are marked in red, where phase identification is distinct. The last four pictures (i)–(l) are taken after pulling is stopped (Color figure online).

D. Initialization of PCG

After 2 hours of growth, the appearance of a second phase band at temperatures below those of the growing s/l interface is presented in Figure 3(a) and marked by the arrow in Figure 2. After 1 hour, a band that coagulated from several bands reached the s/l interface, as shown in Figure 3(b), and began to travel along the former s/l interface. Although the temperatures and concentrations must be considered with care, the coagulated band formed at temperatures below T_p . This fact leads to the conclusion that the lateral and coagulated bands comprise the peritectic β -phase.

As mentioned above, phase-field simulations predicted that island banding leads to PCG if islands spacing falls within a stable lamellar spacings range.^[5] In the present case, several coagulated bands exhibited PCG. In Figure 3(b), a boundary between the two bands (marked in blue) can be observed. At this grain boundary groove, the lateral growth of the peritectic phase along the pro-peritectic interface was interrupted, and a patch of the primary phase remained (Figure 3(c)). In addition, the formation of primary phase patches without the presence of a peritectic phase grain boundary was observed. However, our observations did not confirm the above mentioned prediction.

Note that ECG is initiated by a morphological instability associated with the lateral growth of the secondary phase.^[29] Here, the peritectic phase grows laterally across the primary interface and instability occurs predominantly at the boundaries of the coagulated band, thus leading to these patches. However, the patches shown in Figure 3(c) do not resemble the regular pattern formed by the morphological instability of the secondary-phase interface, as reported in.^[29] In addition, they do not resemble the rapid spread of two-phase growth out of a grain boundary, as reported in.^[30]

E. Progression of PCG

PCG began immediately after the peritectic β -phase traveled along the α /l interface in the following order. It appeared first in larger patches, followed by thin but long lamellae (sometimes with necking), in increasing number of curved lamellae together with rod-like objects, and finally only in rods. This transition occurred over 18 h, and the interface further recoiled from approximately 1.5–1.9 mm to 3.8–4.4 mm from the right edge of the FOV. 3.8–4.4 mm corresponds to an interface temperature of 400–398 K according to Figure 5. At this interface position, surprisingly, both α and β solid phases were still observed in contact with

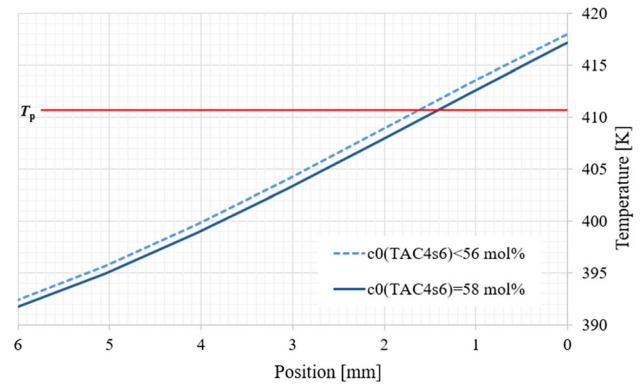


Fig. 5—Temperature along the cartridge axis. The exact values depend on observations made with TAC4s6 and the assumed concentration of this segment. An accuracy of ± 1 K is considered for the predicted temperatures.

the liquid. According to the TRIS–NPG phase diagram (Figure 1), the melting point of β consisting of 100 pct NPG is 401.1 K; therefore, a β /l interface should no longer exist. A possible solution to this contradiction is to assume that an unknown third component opens and lowers the β solidification interval. The origin of that third component is unclear. Most probably, it was introduced from the as-delivered NPG that exhibited only a purity of > 99 pct but also the > 99.9 pct TRIS may have added impurity to the alloy. The assumption of a temperature gradient in the cartridge that is lower than that shown in Figure 5 is less likely as pure β was also observed to leave the left side of the FOV; that would suggest that the temperature on the left side of the FOV must be above 401.1 K. However, this seems less realistic.

A convex curved and inclined s/l interface can be caused either thermally or solutally. A thermal reason is typically permanent, whereas a solutal reason that originates from segregation may vary with time by solute diffusion. From Figure 2, the convex curvature remained almost constant (parallel curves for the center, upper, and lower parts). So it is likely that the cooling from the upper and lower parts of the cartridge was slightly stronger than that from the central part. The cartridges exhibited specific glass spacers on the upper and lower parts (with openings that allowed the material in the center to expand/contract without forming bubbles). The spacers in direct contact with the glass windows might cool slightly faster than the organic material. However, this effect is small and, as outlined above, might cause a temperature difference of less than 0.5 K.

By contrast, Figure 2 shows that the inclination of the interface changed with time, thus indicating that solute diffusion was active. As discussed above, a thermal bias of the TA facility leads to a position difference of 0.2 mm between foremost and backmost interface at the front and the rear window, respectively. However, the interface position difference increased to approximately 5 mm during pulling. During growth, solute rejection at the interface increased both solute concentration in front of the s/l interface and solute diffusion into the

bulk melt. Under steady-state conditions, solute rejection and the diffusion flux away from the interface are balanced, and the interface composition remains constant; consequently, the growth velocity is equal to the pulling velocity. In the present case, the growth velocity was less than the pulling velocity, and the solute pile-up ahead of the interface was ongoing. So, the experiment was still in the initial transient stage.^[31,32] As the s/l interface was inclined, the diffusion profile ahead of the front had a lateral component, which led to the depletion and accumulation of solute at the foremost and backmost fronts, respectively. This phenomenon increased the concentration difference thereby increasing the interface position difference. After stopping the pulling, diffusion in the longitudinal direction reduced the solute pile-up; consequently, the concentration at the interface decreased. Therefore, the interface moved to higher temperatures and lower positions. In addition, the concentration difference along the interface began to balance, and the position difference decreased (until it reached the value given by the thermal bias). The corresponding changes in the interface positions are confirmed by the curves presented in Figure 2.

Another important phenomenon is that the lamellae and rods shifted along the interface toward lower temperatures (see Figures 3(h) through (l), 4(a) through (e)). They grew with some lateral contribution, thus exhibiting the impression that they grew straight with the inclined interface. As such, they increasingly approached the solute-enriched back part of the s/l interface. Thermodynamically, the peritectic β -phase is favored in NPG enriched liquid; the lamellae and rods, which consist of the pro-peritectic α -phase, lose necessary growth conditions and thus disappear when finally reaching the back part of the interface.

Generally, a less solute enriched liquid at the foremost s/l interface favors the formation of the pro-peritectic α -phase, whereas a heavily enriched liquid at the backmost interface favors the peritectic β -phase. Therefore, the cellular instabilities that developed at the foremost part of the interface after 20 hours of growth (Figures 4(g), (h)) might most probably consist of α . After pulling was stopped, these cells became flatter, similar to the α rods observed in the middle part of the interface (Figures 4(i) through (l)). In the last picture (Figure 4(l)), the foremost part of the interface shows the α -phase, and the rearmost part shows the β -phase. Evidently, at temperatures of $399\text{--}400 \pm 1$ K, both phases could form a stable solid/liquid interface. Thus, the unknown third element is suggested to alter the phase diagram such that the β /l two-phase region bends downward, similar to that of the α -liquidus, and around $399\text{--}400$ K, the α /l two-phase overlaps with the β /l two-phase.

V. CONCLUSIONS

In the transparent peritectic model system TRIS–NPG, the formation of PCG began with the occurrence of lateral bands of the peritectic β -phase in the gap between the pro-peritectic α -phase and cartridge

glass window. During the initial transient stage, an inclined α /l interface enriched the solute at the backmost part of the solidifying interface, thus favoring the growth of β . Whether the β -phase nucleated during processing in the α /l mushy region or was present from the beginning is unclear.

However, a necessary condition that enables the β -phase band to reach the α /l interface is that the interface temperature should fall below T_p , at least in some areas (such as the central part of the backmost interface). The recoil of the s/l interface during the initial transient gradually reduced the interface temperature such that β could finally reach the entire α /l interface. However, some larger patches remained in contact with the liquid, and thus, PCG began. As the interface temperature further decreased, the α patches changed into long lamellae, followed by an increasing number of curved lamellae with some rod-like objects. Finally, only rods grew coupled with the β matrix.

In this study, PCG occurring during the initial transient stage is an essential novel aspect compared with the literature. The solute flux across the s/l interface grows as $V(1-k)$ with a redistribution coefficient k .^[31,32] Therefore, the solute amount rejected by the interface is higher for the α -phase than for the β -phase ($k_\alpha < k_\beta$). At steady-state, the flux across the interface is balanced by the diffusion flux in the growth direction and laterally toward the other phase. Thus, the resulting solute profile in the case of steady-state PCG is an exponential decay with some modulation near the interface.^[12,13] However during the initial transient stage, the solute accumulation ahead of the interface first prevents diffusion away from the interface. In addition, the growth velocity only gradually approaches the steady-state velocity; thus, the flux across the interfaces is initially small, and the corresponding lateral modulation weak. As the growth velocity approaches the pulling velocity, the modulation becomes stronger, and the importance of diffusion in the growth direction increases. According to this argument, the diffusion coupling for PCG during initial transient should be weak compared with the fully developed steady-state situation. Additionally, the decreasing interface temperature during the initial transient may lead to a preference for the peritectic phase. During the present μg campaign, in three cases where PCG was observed, the pro-peritectic phase gradually disappeared and the peritectic β -phase prevailed. In the case presented in this study, the concentration difference between the frontmost and backmost interfaces increased during the 22 hours of PCG (increasing interface inclination); thus, the growth conditions were favored for the α - and β -phases at the foremost and rearmost interfaces, respectively.

Unexpectedly, both solid phases contacted the liquid at relatively low interface temperatures. This observation is considered as evidence that an unknown third element modifies the thermodynamically stable region at which β is in equilibrium with the liquid. We suggest that the modified solidification interval of β should follow the liquidus line of α such that the metastable α solidification interval (estimated using the CALPHAD

approach) overlaps with the modified β solidification interval.

ACKNOWLEDGMENTS

This research was supported by the ESA in the framework of the project METCOMP, and by the Austrian Research Promotion Agency (FFG) under Grant Number 865969. We also thank Michael Spreitzhofer for his assistance in measuring a large number of interface positions.

FUNDING

Open access funding provided by Montanuniversität Leoben.

CONFLICT OF INTEREST

On behalf of all authors, the corresponding author states that there is no conflict of interest.

OPEN ACCESS

This article is licensed under a Creative Commons Attribution 4.0 International License, which permits use, sharing, adaptation, distribution and reproduction in any medium or format, as long as you give appropriate credit to the original author(s) and the source, provide a link to the Creative Commons licence, and indicate if changes were made. The images or other third party material in this article are included in the article's Creative Commons licence, unless indicated otherwise in a credit line to the material. If material is not included in the article's Creative Commons licence and your intended use is not permitted by statutory regulation or exceeds the permitted use, you will need to obtain permission directly from the copyright holder. To view a copy of this licence, visit <http://creativecommons.org/licenses/by/4.0/>.

REFERENCES

1. W. Kurz and P.R. Sahn: *Gerichtet Erstarrte Eutektische Werkstoffe*, Springer, Berlin, 1975.

2. J.-H. Lee and J.D. Verhoeven: *J. Cryst. Growth*, 1994, vol. 144, pp. 353–366.
3. M. Vandyoussefi: Ph.D. Thesis, Ecole Polytechnique Fédérale de Lausanne, CH, 1997.
4. M. Vandyoussefi, H.W. Kerr, and W. Kurz: *Acta Mater.*, 2000, vol. 48, pp. 2297–06.
5. T.S. Lo, S. Dobler, M. Plapp, A. Karma, and W. Kurz: *Acta Mater.*, 2003, vol. 51, pp. 599–611.
6. S. Dobler, T.S.S. Lo, M. Plapp, A. Karma, and W. Kurz: *Acta Mater.*, 2004, vol. 52, pp. 2795–08.
7. J. Vallotton, J.A. Dantzig, M. Plapp, and M. Rappaz: *Acta Mater.*, 2013, vol. 61, pp. 5549–60.
8. B. Chalmers: *Physical Metallurgy*, Wiley, New York, 1959.
9. B. Chalmers: *Principles of Solidification*, Wiley, New York, 1964.
10. J. Livingston: *Mater Sci Eng*, 1971, pp. 61–70.
11. M.C. Flemings: *Solidification Processing*, McGraw-Hill, New York, 1974.
12. W.J. Boettinger: *Met. Trans.*, 1974, vol. 5, pp. 2023–31.
13. K.A. Jackson and J.D. Hunt: *Trans. AIME*, 1966, vol. 237, pp. 843–852.
14. K.A. Jackson and J.D. Hunt: *Trans. AIME*, 1966, vol. 236, pp. 1129–41.
15. R. Trivedi: *Met. Mater. Trans. A*, 1995, vol. 26, pp. 1583–90.
16. J.-S. Park and R. Trivedi: *J. Cryst. Growth*, 1998, vol. 187, pp. 511–15.
17. P. Mazumder, R. Trivedi, and A. Karma: *Met. Mater. Trans. A*, 2000, vol. 31, pp. 1233–46.
18. A. Ludwig, J.P. Mogeritsch, and T. Pfeifer: *Acta Mater.*, 2017, vol. 126, pp. 329–35.
19. M. Barrio, D.O. Lopez, J.L. Tamarit, P. Negrier, and Y. Haget: *J. Mater. Chem.*, 1995, vol. 5, pp. 431–39.
20. S. Santos-Moreno, S. Doppiu, G.A. Lopez, N. Marinova, Á. Serrano, E. Silveira, and E.P. del Barrio: *Materials (Basel)*, 2020, vol. 13, pp. 1–22.
21. R. Shi, D. Chandra, A. Mishra, A. Talekar, M. Tirumala, and D.J. Nelson: *Calphad*, 2017, vol. 59, pp. 61–75.
22. A. Ludwig, J. Mogeritsch, and V.T. Witusiewicz: *J Cryst. Growth*, 2023, vol. 604, 127052.
23. A. Ludwig and J. Mogeritsch: *IOP Conf. Ser. Mater. Sci. Eng.*, 2023, vol. 1274, 012032.
24. A. Ludwig and J.P. Mogeritsch: *Scripta Mater.*, 2023, p. submitted.
25. A. Ludwig, J. Mogeritsch, M. Kolbe, G. Zimmermann, L. Sturz, N. Bergeon, B. Billia, G. Faivre, S. Akamatsu, S. Bottin-Rousseau, and D. Voss: *JOM*, 2012, vol. 64, pp. 1097–101.
26. W.G. Pfann: *AIME*, 1955, vol. 203, pp. 961–64.
27. W.A. Tiller: *J. Appl. Phys.*, 1963, vol. 34, pp. 2757–769.
28. D.J. Allen and J.D. Hunt: in *Int. Conf. Solidification and Casting, I. London: Institute of Metals*, 1977, pp. 39–43.
29. S. Akamatsu, S. Moulinet, and G. Faivre: *Metall. Mater. Trans. A Phys. Metall. Mater. Sci.*, 2001, vol. 32, pp. 2039–48.
30. M. Serefoğlu and R.E. Napolitano: *Acta Mater.*, 2011, vol. 59, pp. 1048–057.
31. W. Kurz and D.J. Fisher: *Fundamental of Solidification*, 4th ed. Trans. Tech. Publ, Aedermansdorf, 1998.
32. J.A. Dantzig and M. Rappaz: *Solidification*, 2nd ed. EPFL Press, Lausanne, 2016.

Publisher's Note Springer Nature remains neutral with regard to jurisdictional claims in published maps and institutional affiliations.